Interferometric measurement of high-frequency density fluctuations in Madison symmetric torus

Y. Jiang and D. L. Brower
Electrical Engineering Department, and Institute of Plasma and Fusion Research, University of California, Los Angeles, California 90095

N. E. Lanier
Department of Physics, University of Wisconsin-Madison, Madison, Wisconsin 53706

(Presented on 9 June 1998)

As a consequence of recent improvements to the far-infrared (FIR) interferometer time response, from bandwidth of 10 kHz up to 1 MHz, high-frequency density fluctuations can now be resolved on the Madison symmetric torus (MST) reversed-field pinch. The phase measurement allows absolute calibration of the fluctuation amplitude while eleven chords generate information on the spatial distribution. Density fluctuations up to 200 kHz are observed. A unique feature of the MST interferometer is that six chords are toroidally displaced 5° from the remaining five. Hence, besides information on the poloidal structure, i.e., $m=1$, toroidal information is also available. By computing the cross power, coherence, and cross phase between two toroidally displaced chords, one can determine the toroidal rotation speed, dispersion, and correlation length. © *1999 American Institute of Physics.* [S0034-6748(99)58001-5]

I. INTRODUCTION

The Madison symmetric torus (MST) is a reversed field pinch whose experimental program includes a focus on basic physics studies of fluctuations and transport. A multichannel far-infrared interferometer was installed and operated beginning in 1992 for the purpose of characterizing the electron density profile and its evolution throughout the various confinement regimes of MST.[1] Recently, through implementation of digital phase detection techniques,[2] the time response has been improved by two orders of magnitude thereby permitting detection of high-frequency electron density fluctuations. Since the confinement on MST has been shown to be limited by turbulence, both electrostatic and electromagnetic, investigation of these fluctuations is crucial to the overall experimental program. This article will describe how an interferometric measurement of the electron density can be utilized to characterize turbulent fluctuation parameters such as amplitude, spatial distribution, frequency and wave number spectrum, dispersion, and coherence length. The high-speed interferometer is also capable of resolving fast plasma events such as the sawtooth collapse.[2]

II. INTERFEROMETER SYSTEM

MST is a reversed field pinch with torus major radius $R_0=150$ cm and minor radius $a=52$ cm which operates with plasma currents up to 500 kA and electron densities of $n_{eo}=1.5\times10^{13}$ cm^{-3} for discharge pulse lengths up to 100 ms. The multichannel, vertically viewing, heterodyne FIR laser interferometer consists of eleven chords divided between toroidal locations 250° (five chords located at $x=R-R_0=36$, 21, 6, -9 and -24 cm) and 255° (six chords located at $x=43$, 28, 13, -2, -17, -32 cm). The eleven individual chords access the plasma through 3.8 cm diameter holes in the vacuum vessel. The laser system operates at a frequency of 694 GHz (432.5 μm) with difference frequency IF between the dual laser cavities typically set to 750–1000 kHz. Further details of the system hardware have previously been described.[1]

The frequency bandwidth of the interferometer system has been increased from the analog limit of <10 kHz to 1 MHz through implementation of a digital phase comparator technique. In this approach, the probe and reference waveforms are directly digitized and the phase is computed in software using a numerical demodulation algorithm.[2] The upper bound on the system bandwidth is determined by the laser IF frequency. For data shown here, the IF frequency was set to 750 kHz and sampled at 1 MHz. This results in an aliasing of the IF down to 250 kHz which becomes the effective system bandwidth. This bandwidth is sufficient for turbulence studies on MST, where the fluctuation power is commonly below 150 kHz. By reducing the sampling rate and aliasing the IF, the total system data load is minimized while invoking no loss of information.

The sensitivity of the interferometric fluctuation measurement to the wave number is determined by the shape and orientation of the sample volume (a vertical chord with 3.8 cm diameter) with respect to the plasma modes. A vanishingly small sample volume would be sensitive to all wave numbers. An upper bound on the sensitivity to the wave number in a particular direction can be defined when the sample volume length in that direction is half a wavelength, i.e., $k_{\max}=2\pi/\lambda_{\max}=\pi/L$, where L is the sample volume dimension. For a vertical chord, for directions transverse to the beam, the wave number limit is $k_{\max}\simeq0.8$ cm^{-1} while along the beam the upper bound is 0.05 cm^{-1} for the shortest chord and 0.03 cm^{-1} for the longest chord.

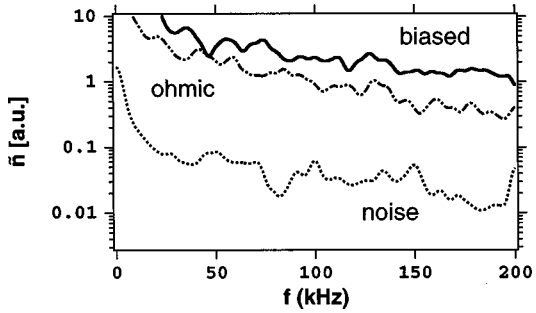

FIG. 1. Typical power spectra for an interferometer chord.

For the outer half of minor radius on MST, $r>a/2$, perpendicular corresponds to the toroidal and radial directions while the parallel corresponds to the poloidal direction. This stems from the fact that the toroidal and poloidal fields are of comparable magnitudes and the device safety factor q is always much less than 1. Consequently, edge interferometer chords are equally sensitive to both radial and toroidal wave numbers while the central chords see only the toroidal component. The radial component is cutoff due to the extended sample volume length. The fluctuation poloidal component is observed for all chord positions.

As the interferometer operates on the basis of a phase measurement technique, absolute calibration of the measured phase change due to the plasma density and its fluctuations is easily achieved. The eleven interferometer chords provide eleven line-integrated measurements of $\int n_e dl$ where $n_e = \bar{n}_e + \tilde{n}_e$, the average and fluctuating quantities. These in turn can be inverted to provide information on the local density and density fluctuation distribution.

III. APPLICATIONS TO MST

For the digital phase comparator technique described previously, the detector output from the reference and plasma legs of the interferometer is directly digitized using a LeCroy 6810 waveform recorder [12 bit] with 5 MHz bandwidth and variable sampling speed up to 5 MHz. Sampling speed for these data was set to 1 MHz. Low-pass filtering at 200 kHz has been applied to the results described below.

In Fig. 1, the frequency power spectra, averaged over 1.5 ms, for typical chord-averaged data are shown. Both the ohmic plasma result and that for external electrostatic biasing show a broadband spectra well above the noise level out to 200 kHz. The fluctuation level peaks at low frequencies ($f<20$ kHz) with the overall amplitude being larger for the case with external biasing. Similar results are available from all the interferometer chords.

Density fluctuation time traces for the 255° and 250° toroidal locations from 15.4 to 15.6 ms are shown in Figs. 2(a) and 2(b), respectively. A sawtooth crash occurs at approximately 15.54 ms. The high-frequency oscillations with period roughly 10 μs are out-of-phase for the two toroidal locations. Further expansion of these plots, as shown in Figs. 2(c) and 2(d), reveals a phase delay within each toroidal location. These delays are plotted against time and chord position in Fig. 3. For a given toroidal position, the slope

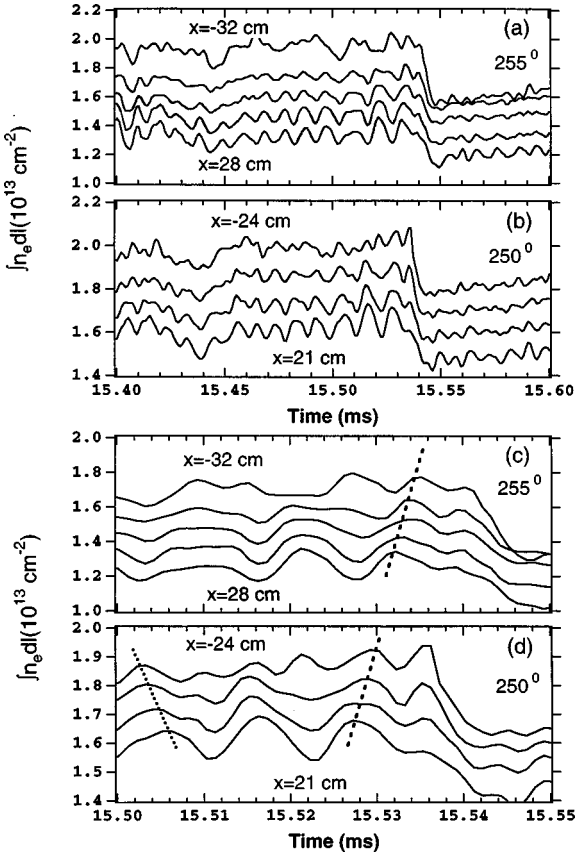

FIG. 2. Interferometer time traces for toroidal locations (a) 255° and (b) 250°. Expanded time traces for toroidal locations (c) 255° and (d) 250°. The dashed line in (c) and (d) connects maxima showing a time delay from chord to chord.

provides an estimate of the poloidal (or parallel) velocity which is 230 km/s. When comparing chords from different toroidal locations, the time delay divided by toroidal separation generates an estimate of the toroidal velocity which is 28 km/s. These measurements of velocity are made in the laboratory-frame-of-reference. For the poloidal velocity estimate, the slope can change sign when going from one perturbation to the next [see Fig. 2(d)]. This most likely results from the chord-averaged nature of the measurement, as poloidally propagating fluctuations located above and below the midplane along the same chord would be observed to propagate in opposite directions.

Information on the fluctuation propagation velocity across the entire spectrum, as opposed to a specific frequency, can be obtained by computing the coherence and

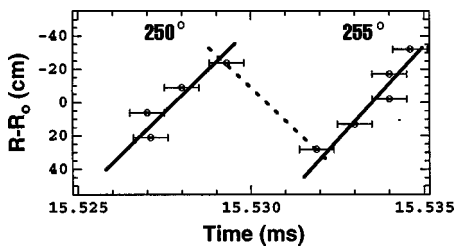

FIG. 3. Plot of delay time vs chord position for data from 255° to 250° toroidal locations.

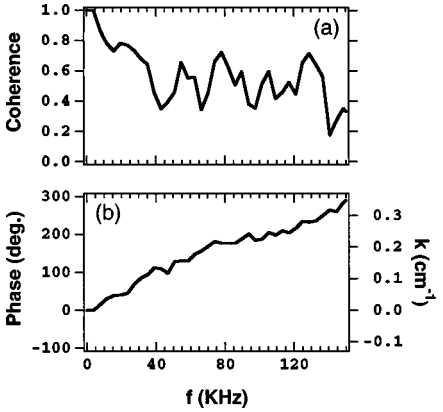

FIG. 4. Computed (a) coherence and (b) cross phase (or dispersion) between two toroidally separated chords at $x=13$ and 21 cm. Toroidal separation is 15 cm.

cross phase between two toroidally separated chords as shown in Fig. 4. Across most of the spectrum, out to 150 kHz, the coherence is approximately 0.4, well above the statistical noise level of 0.1. This indicates that the fluctuation toroidal correlation length is of order or greater than the toroidal separation for this externally biased plasma. The cross-phase plot shows a linear variation with a frequency out to 150 kHz. As done with two-point correlation techniques, dividing the cross phase by the toroidal separation provides an estimate of the wave number, toroidal wave number in this case, versus frequency or the fluctuation statistical dispersion. For the 100 kHz oscillation discussed in the previous paragraph, the corresponding toroidal wave number is 0.23 cm^{-1} with phase velocity 27 km/s. In addition, the poloidal mode number $k_\theta = 0.03\ \mathrm{cm}^{-1}$ indicating $k_\parallel / k_\perp \ll 1$. This value of the toroidal wave number is well below the system limit of 0.8 cm^{-1} and the estimated phase velocity agrees well with that determined from Fig. 3. The toroidal wave number can be related to the toroidal mode number n by the expression $k_\phi = n/R$ which gives $n=38$ for the 100 kHz fluctuation. If the sign of the externally biasing voltage is changed, the fluctuation propagation direction also reverses, as expected if the measured velocity is dominated by $E\times B$ effects when compared to the actual mode velocity in the plasma frame.

On MST, analysis of the magnetic fluctuations has shown that the modes which dominate transport in the core correspond to $n=5-10$. This would correspond to the frequency range of 13–26 kHz in Fig. 4. This portion of wave number and frequency space is easily resolved by the high-speed interferometer system and actually corresponds to the region of the largest measured density fluctuations. Previously on ZT-40M, an infrared interferometer system was used to investigate density fluctuations. However, there was no toroidal displacement of the chords thereby precluding any information on the toroidal mode number.[3]

An estimate of the poloidal correlation length can be obtained by examining the changes in coherence versus chord separation, at the same toroidal position, as shown in Fig. 5. For this ohmic plasma, the coherence drops to or below 0.2 across most of the spectrum for chords separated

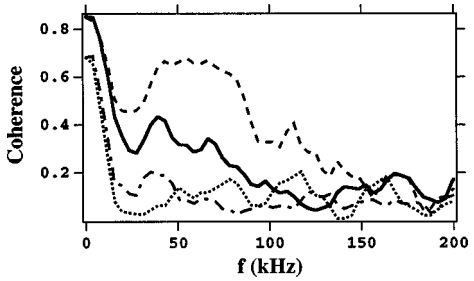

FIG. 5. Coherence change with chord separation; $\delta x = 15$ cm (dashed line), 30 cm (solid line), 45 cm (short dashed-long dashed line), and 60 cm (short dashed line).

along the major radius by 45 cm. If the fluctuations originate largely from the edge of the plasma, this would correspond to a poloidal separation or coherence length $l_\theta \approx 45$ cm. If we define the width of the spectrum as $\sigma_k = \sqrt{2}/l_\theta$, this would correspond to $\sigma_k = 0.03\ \mathrm{cm}^{-1}$. When computing the cross phase for two edge chords, located on opposite sides of the magnetic axis, the observed phase difference is π for frequencies above ≈ 5 kHz indicating the poloidal mode number is $m=1$. Lower frequencies are in phase suggesting $m=0$.

Information on the density fluctuation spatial distribution can be obtained by integrating the power spectra over the

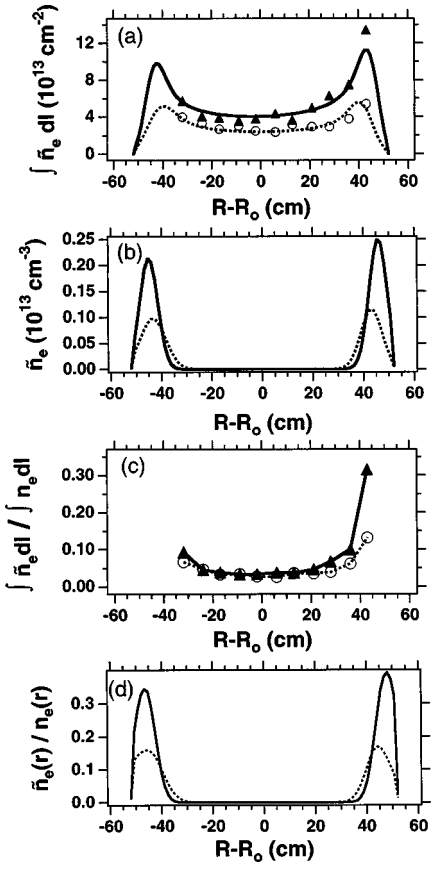

FIG. 6. Density fluctuation spatial distribution (a) line-integrated $\int \tilde{n}(x)dl$, (b) inverted $\tilde{n}(x)$, (c) line-integrated fractional fluctuation level $\int \tilde{n}(x)dl / \int \overline{n}(x)dl$, and (d) local fractional fluctuation level. Solid data points/lines correspond to externally biased plasmas and open, (dashed) data points, (lines) correspond to ohmic discharges.

desired frequency range and plotting the resultant amplitude against the chord position. In Fig. 6(a), this is done over the frequency band from 50 to 150 kHz for biased and unbiased plasma discharges as shown by the discrete data points. The power spectra for each chord were evaluated over a 1 ms time window. For both plasma cases, the line-integrated fluctuation profile $\int \tilde{n}(x)dl$ is slightly hollow. This is contrary to the line-integrated mean density profile $\int \overline{n}(x)dl$ which is centrally peaked indicating a peaked inverted profile. The density fluctuations are observed to be larger for the case of the biased plasma.

The line-integrated density fluctuation profile can also be inverted by making the assumption that the fluctuation distribution is symmetric above and below the torus midplane. As is the case for the mean density profile, no assumption regarding in/out symmetry need be made. Since we are inverting only the fluctuation amplitude, averaged over a time interval long compared to the fluctuation frequency, the above assumptions seem reasonable. Coherent oscillations 180° out-of-phase, like an $m=1$ oscillation picked up by the central chord at the plasma top and bottom, will average to zero producing no signal. However, for this to occur, a poloidal correlation length much greater than the earlier estimate of 45 cm is required. Inversion of the fits to the data points in Fig. 6(a) gives the local density fluctuation profiles shown in Fig. 6(b). In each case, with and without external biasing, the fluctuation distribution is estimated to be strongly peaked at the edge. This is as expected for a hollow line-integrated profile. The region of space where the fluctuation amplitude peaks also corresponds to the steep density gradient region of the plasma density profile. Care must be taken when fitting the line-integrated data before inversion as the number of spatial points is limited, especially at the edge. However, despite this limitation, these data provide a good indication of what one might expect the fluctuation distribution to look like.

Another way to view the amplitude data is by dividing the fluctuating line integral by the mean line integral in order to generate an estimate of the line-integrated fractional fluctuation level as seen in Fig. 6(c). Once again the profile is edge peaked with a line-integrated fluctuation level of 30% for the outermost chord. The local fractional fluctuation level is obtained by dividing $\tilde{n}_e$ [Fig. 6(b)] by the local density as shown in Fig. 6(d). Once again we see that the density fluctuation distribution is strongly peaked near the plasma edge. The fluctuation profile information plotted in Fig. 6 can be produced every $\approx$0.5 ms for a specified frequency band. This enables temporal tracking of the fluctuation amplitude and spatial distribution through confinement transitions on MST.

IV. CONCLUSION

In summary, by use of digital techniques for evaluating the interferometer phase information, the time response of the system was decreased by 10^2 thereby allowing investigation of high-frequency electron density fluctuations. For the eleven chords making up the MST FIR interferometer system, one can now evaluate the frequency and wave number spectra, dispersion, correlation lengths, and fluctuation spatial distribution throughput the discharge pulse length. This upgraded system will be utilized to investigate density fluctuations in the various improved confinement regimes available on MST.

ACKNOWLEDGMENT

This research is supported by the U.S. Department of Energy under Grant DE-FG03-86ER-53225, Task III.

[1] S. R. Burns, W. A. Peebles, D. Holly, and T. Lovell, Rev. Sci. Instrum. **63**, 4993 (1992).
[2] Y. Jiang, D. L. Brower, L. Zeng, and J. Howard, Rev. Sci. Instrum. **68**, 902 (1997).
[3] M. G. Rusbridge and A. R. Jacobson, J. Appl. Phys. **56**, 757 (1984).